Structural basis for basal activity and autoactivation of abscisic acid (ABA) signaling SnRK2 kinases

Ley-Moy Ng[a,b,1], Fen-Fen Soon[a,b,1], X. Edward Zhou[a,1], Graham M. West[c], Amanda Kovach[a], Kelly M. Suino-Powell[a], Michael J. Chalmers[c], Jun Li[a,b], Eu-Leong Yong[b], Jian-Kang Zhu[d,2], Patrick R. Griffin[c], Karsten Melcher[a,2], and H. Eric Xu[a,e,2]

[a]Laboratory of Structural Sciences, Van Andel Research Institute, Grand Rapids, MI 49503; [b]Department of Obstetrics and Gynecology, National University Hospital, Yong Loo Lin School of Medicine, National University of Singapore, Singapore; [c]Department of Molecular Therapeutics, Translational Research Institute, The Scripps Research Institute, Scripps Florida, Jupiter, FL 33458; [d]Department of Horticulture and Landscape Architecture, Purdue University, West Lafayette, IN 47907; and [e]Van Andel Research Institute–Shanghai Institute of Materia Medica Center, Center for Structure and Function of Drug Targets, State Key Laboratory of Drug Research, Shanghai Institute of Materia Medica, Shanghai Institutes for Biological Sciences, Chinese Academy of Sciences, Shanghai 201203, People's Republic of China

Contributed by Jian-Kang Zhu, November 17, 2011 (sent for review October 18, 2011)

Abscisic acid (ABA) is an essential hormone that controls plant growth, development, and responses to abiotic stresses. Central for ABA signaling is the ABA-mediated autoactivation of three monomeric Snf1-related kinases (SnRK2.2, -2.3, and -2.6). In the absence of ABA, SnRK2s are kept in an inactive state by forming physical complexes with type 2C protein phosphatases (PP2Cs). Upon relief of this inhibition, SnRK2 kinases can autoactivate through unknown mechanisms. Here, we report the crystal structures of full-length *Arabidopsis thaliana* SnRK2.3 and SnRK2.6 at 1.9- and 2.3-Å resolution, respectively. The structures, in combination with biochemical studies, reveal a two-step mechanism of intramolecular kinase activation that resembles the intermolecular activation of cyclin-dependent kinases. First, release of inhibition by PP2C allows the SnRK2s to become partially active because of an intramolecular stabilization of the catalytic domain by a conserved helix in the kinase regulatory domain. This stabilization enables SnRK2s to gain full activity by activation loop autophosphorylation. Autophosphorylation is more efficient in SnRK2.6, which has higher stability than SnRK2.3 and has well-structured activation loop phosphate acceptor sites that are positioned next to the catalytic site. Together, these data provide a structural framework that links ABA-mediated release of PP2C inhibition to activation of SnRK2 kinases.

Abscisic acid (ABA) is a key hormone that plants use to regulate many important physiological processes, including seed germination and bud dormancy. ABA is also the central regulator to protect plants against abiotic stresses such as drought, cold, and salinity, which are the principal causes for crop losses worldwide (1). At the center of the ABA signaling network are the three Snf1-related kinases, SnRK2.2, -2.3, and -2.6 (2, 3), the kinase domains of which have high sequence homology to mammalian AMP-activated kinase (AMPK) and its yeast homolog Snf1 (*SI Appendix*, Fig. S1*A*). SnRK2.6/OST1 (open stomata 1) is critically important for the ABA-induced closure of stomata in response to drought. SnRK2.2 and SnRK2.3, which are functionally redundant and share almost identical sequences, are predominantly responsible to transduce the ABA response to the inhibition of seed germination and seedling growth. snrk2.2/2.3/2.6 triple mutants are severely compromised in all known ABA responses, implying their collectively essential role in ABA signaling (4). In addition to the conserved kinase domain, SnRK2 kinases contain a C-terminal regulatory region that encompasses two conserved motifs: (*i*) the SnRK2 box, which is required for kinase activity by an unknown mechanism; and (*ii*) the highly acidic ABA box, which is important to mediate SnRK2 interactions with type 2C protein phosphatases (PP2Cs) (*SI Appendix*, Fig. S1*A*) (5, 6).

The ABA signal is transmitted through a conserved core pathway that culminates in activation of SnRK2 kinases through inhibition of PP2Cs by ABA-bound receptors (*SI Appendix*, Fig. S1*B*) (7, 8). In the absence of ABA, the SnRK2 kinases are inactivated by clade A PP2Cs, including Homology to ABI1/ABI2 (HAB1) (3, 9–11), which physically interact with SnRK2 kinases and dephosphorylate a critical serine residue in the kinase activation loop (5, 6, 12). The presence of the ABA signal is perceived by the PYR/PYL/RCAR family of START domain receptors (10, 11). Upon ABA binding, these receptors undergo a conformational change that allows them to bind to the catalytic site of PP2Cs and inhibit their enzymatic activity (9, 13–16). In turn, ABA-induced inhibition of PP2Cs leads to autoactivation of SnRK2 kinases by activation loop autophosphorylation, which allows the SnRK2s to relay the ABA signal into several distinct pathways, leading to transcriptional activation, ion channel regulation, and generation of second messengers (*SI Appendix*, Fig. S1*B*) (7, 8). Recent structural studies have unraveled detailed molecular mechanisms of agonism and antagonism of ABA receptors, as well as receptor-mediated inhibition of PP2Cs (9, 13–19), but the mechanisms of SnRK2 autoactivation remain unclear.

Results

SnRK2 Kinases Have Basal, Phosphorylation-Independent Activity That Is Greatly Increased by Activation Loop Phosphorylation. To characterize biochemical functions of SnRK2 kinases, we purified full-length SnRK2.2, -2.3, and -2.6 as recombinant proteins and determined their phosphorylation status by mass spectrometry. In agreement with a previous study on recombinant SnRK2.6 (5), we found clear evidence for phosphorylation of Ser7, Ser29, Ser175, and Thr176 (*SI Appendix*, Fig. S2*A*). Mutational studies have indicated that phosphorylation of Ser175 in the SnRK2.6 activation loop (5, 6, 12), but not of Ser7, Ser29, or Thr176 (5), is required for full activity of recombinant SnRK2.6. In SnRK2.2 and -2.3, the residues corresponding to Ser29 were phosphorylated as well, whereas phosphorylation of the residues corresponding to the critical Ser175 in SnRK2.2 (Ser177) and SnRK2.3 (Ser176) was below the limit of detection in the absence of ATP incubation (*SI Appendix*, Figs. S2*A* and S3) and low in the presence of ATP incubation (*SI Appendix*, Fig. S2*B*). Consistent with these data, the level of SnRK2.6 autophosphorylation upon incubation with ATP is higher by a factor of ~5–10 than that of SnRK2.2 and 2.3 as determined by [^{32}P]-γATP labeled proteins in SDS gels even though the activation

Author contributions: J.L., E.-L.Y., J.-K.Z., P.R.G., K.M., and H.E.X. designed research; L.-M.N., F.-F.S., X.E.Z., G.M.W., A.K., K.M.S.-P., M.J.C., K.M., and H.E.X. performed research; L.-M.N., F.-F.S., X.E.Z., G.M.W., A.K., K.M.S.-P., M.J.C., P.R.G., K.M., and H.E.X. analyzed data; and K.M. and H.E.X. wrote the paper.

The authors declare no conflict of interest.

Data deposition: The atomic coordinates reported in this paper have been deposited in the Protein Data Bank, www.pdb.org (PDB ID codes 3UC3 and 3UC4).

[1]L.-M.N., F.-F.S., and X.E.Z. contributed equally to this work.

[2]To whom correspondence may be addressed. E-mail: jkzhu@purdue.edu, karsten.melcher@vai.org, or eric.xu@vai.org.

This article contains supporting information online at www.pnas.org/lookup/suppl/doi:10.1073/pnas.1118651109/-/DCSupplemental.

PLANT BIOLOGY

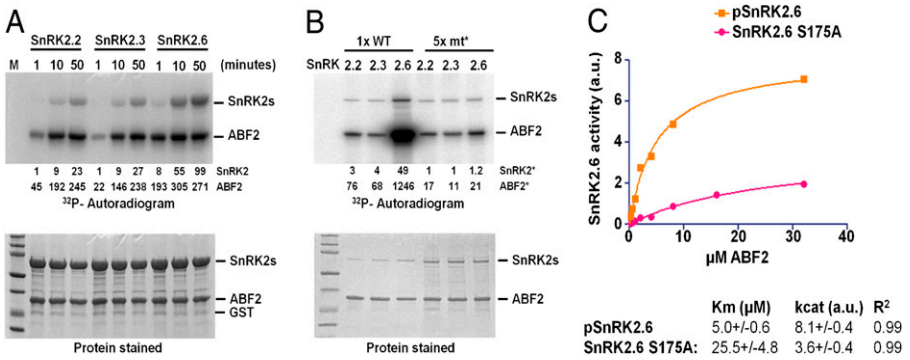

Fig. 1. Biochemical analysis of SnRK2 kinases. (*A*) Time course of SnRK2 auto- and transphosphorylation. Recombinant SnRK2.2, -2.3, and -2.6 were incubated with a fragment of the transcription factor ABF2 (GST-ABF2[73-120]) and with [^{32}P]-γATP for the indicated length of time. Reactions were terminated by boiling in SDS sample buffer, separated by SDS/PAGE, and subjected to autoradiography. Numbers below autoradiogram: densitometry of autophosphorylation (top) and GST-ABF2(73-120) (bottom) phosphorylation bands. M, marker. (*B*) SnRK2 phosphorylation mutants retain basal kinase activity. To accommodate for the high activity of WT SnRK2.6, 0.4 μM WT SnRK2s and 2 μM, each, of SnRK2.2 S177A, 2.3 S176A, and 2.6 S175A mutated (mt) kinases were incubated with GST-ABF2(73-120) and [^{32}P]-γATP for 30 min. *Reactions were separated by SDS/PAGE and subjected to autoradiography. Numbers below autoradiogram: densitometry of autophosphorylation (top) and GST-ABF2(73-120) (bottom) phosphorylation bands normalized for the amount of SnRK2. (*C*) Kinetic analyses of autophosphorylated SnRK2.6 (pSnRK2.6) and SnRK2.6 phosphorylation mutant (S175A). pSnRK2.6 was preincubated for 1 h with 1 mM ATP before dilution and incubation with ABF2 substrate.

loops are identical between SnRK2.3 and 2.6 (Fig. 1*A*, top band). We conclude that all three ABA-signaling SnRK2s can autophosphorylate the central serine residue in the activation loop but that the efficiency of activation loop autophosphorylation varies greatly between SnRK2.6 and SnRK2.2/2.3.

Both SnRK2.2 and -2.3 can phosphorylate a fragment from the transcription factor ABA response element-binding factor (ABF)2 (2, 3), which is a natural substrate of SnRK2 kinases (20, 21), with an activity that is reduced by a factor of 5–10 relative to SnRK2.6 (compare the 10 min data of SnRK2.2 and 2.3 with the 1 min data of SnRK2.6 in Fig. 1*A*), suggesting that autophosphorylation is important for kinase activity. To corroborate this finding, we purified recombinant mutants of the three SnRK2 kinases in which the critical serine residue in the activation loop is replaced by alanine. As shown in Fig. 1*B*, the level of autophosphorylation of SnRK2.2/2.3 and SnRK2.6 is decreased by factors of 3–4 and ~40, respectively, after normalization for the amount of proteins (Fig. 1*B*, bottom). The activity to phosphorylate ABF2 by the mutated kinases is also correspondingly decreased, particularly for SnRK2.6 S175A, which retains only ~2% of WT kinase activity. We also analyzed the kinetic effects of activation loop phosphorylation by determining K_m and k_{cat} for both autophosphorylated SnRK2.6 (pSnRK2.6) and SnRK2.6 S175A. As shown in Fig. 1*C*, autophosphorylation increased the catalytic activity of SnRK2.6 by a factor of >10 (k_{cat}/K_m = 11.3), further supporting the critical role of this serine residue for autophosphorylation and kinase activation. In contrast to the nonphosphorylatable activation-loop serine mutants, SnRK2s are completely inactive in the presence of high concentrations of the PP2C HAB1 (*SI Appendix*, Fig. S2*C* and Ref. 22). Taken together, all three kinases have a similarly high level of phosphorylation-independent basal activity. In contrast, the level of autophosphorylation differs between the kinases and correlates with full kinase activity.

Activation Loop Autophosphorylation Is Likely to Occur Both Inter- and Intramolecularly. Activation loop autophosphorylation is a widespread mechanism for kinase activation and can occur either intermolecularly (in *trans*) or intramolecularly (in *cis*) (23). To determine the mode of SnRK2 autophosphorylation, we generated six different catalytically inactive SnRK2.6 mutants. These mutants are unable to *cis*- (and *trans*-) autophosphorylate (*SI Appendix*, Fig. S4), yet their WT activation loops are expected to still be capable of being *trans*-phosphorylated. We expressed and purified WT and SnRK2.6 mutants with two different tags to allow us to distinguish the two proteins by size. When both proteins were mixed and incubated with [^{32}P]-γATP, both WT and mutant SnRK2.6 proteins were phosphorylated (*SI Appendix*, Fig. S4*B*). This clearly demonstrates that SnRK2s can autophosphorylate in *trans*. Because the activation loops are identical between WT and mutant SnRK2s, we expected at least some mutant SnRK2s to become *trans*-phosphorylated with similar efficiency as WT SnRK2.6. However, the six mutant proteins with single amino acid replacements of key residues in the Mg^{2+}-binding loop (D160R, F161A, and G162A), the ATP-binding loop (G33R), or the catalytic loop (D140A and K142A) were all to the same degree (by a factor of 1.6–2.2) less efficiently phosphorylated than the WT proteins, suggesting that autophosphorylation may occur both in *trans* and in *cis* (*SI Appendix*, Fig. S4*B*). As has been demonstrated for p21-activated protein kinase (PAK)2 kinase (24), autophosphorylation may be initiated in *cis* and then propagated in *trans*.

Crystal Structures of SnRK2.3 and SnRK2.6 Reveal Canonical Kinase Folds. To determine the mechanism of autophosphorylation and high basal activity of SnRK2 kinases, we solved the crystal structures of SnRK2.3 by molecular replacement with the kinase domain of human AMPK α2 (25) (2H6D) as an initial model and the structure of SnRK2.6 using the SnRK2.3 structure as model. In addition, we analyzed their dynamic properties by hydrogen/deuterium exchange (HDX), followed by mass spectrometry, which has become a powerful technique to determine stability and flexibility of proteins and protein–protein interactions (26). WT SnRK2.6 did not crystallize under any condition tested, whereas SnRK2.3 yielded crystals under a single condition that diffracted poorly even after extensive optimization. Introduction of localized surface entropy-reduction mutations (27, 28) allowed us to crystallize and solve the structure of SnRK2.6 D59A/E60A at a resolution of 2.3 Å and of SnRK2.3 D57A/K58A at 1.9 Å (statistics of structure refinement shown in *SI Appendix*, Table S2). The above crystallization mutations lie at the crystal packing interface and do not affect SnRK2 kinase activity or its binding and inhibition by HAB1 (*SI Appendix*, Fig. S5). In the crystal structures, the nonphosphorylated SnRK2.3 and -2.6 adopted canonical bilobal kinase folds very similar to those of AMPK and the yeast AMPK homolog Snf1 (25, 29, 30). A standout feature is the well-ordered SnRK2 box, which forms a single α-helix and is packed parallel against the αC-helix in the N-terminal lobe (Fig.

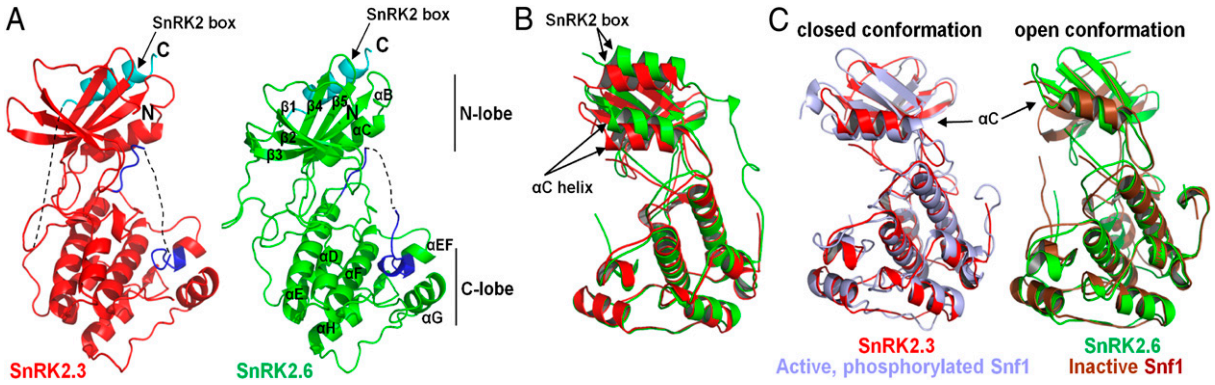

Fig. 2. SnRK2.3 and 2.6 structures. Structure overview of SnRK2.3 and 2.6 monomer A (for monomer B see *SI Appendix*, Fig. S6). (*A*) The SnRK2 boxes are highlighted in cyan, and the activation loop segment is highlighted in blue. Parts that are not resolved in the structures are the C-terminal 44 residues harboring the ABA box and the segments indicated by dotted lines. (*B*) Overlay of the SnRK2.3 (red) and 2.6 (green) structures, indicating that SnRK2.3 and SnRK2.6 adopt closed and open conformations, respectively. (*C*) Overlays of SnRK2.3 (red) with the active Snf1 kinase domain (light blue) (PDB code 3DAE) and of SnRK2.6 (green) with the kinase domain of Snf1 in the inactive, open conformation (brown) (PDB code 2FH9). The SnRK2 boxes were omitted from the overlay for clarity.

2*A*). Not visible in the SnRK2.3 structure were the N-terminal 10 aa, the activation loop, a 4-aa segment between the αF- and αG-helices, the linkers to both sides of the SnRK2 box, and the entire ABA box. SnRK2.6 appears to be more stable and contains more structural elements, including parts of the activation loop and the linker between the kinase domain and the SnRK2 box (Fig. 2*A* and *SI Appendix*, Fig. S6). In perfect agreement with the HDX data, the structured and unstructured regions in the crystal structures match well with the conformational flexibility map of SnRK2.6 kinase generated by HDX analysis (*SI Appendix*, Fig. S7).

Catalytic Centers of SnRK2.3 and -2.6 Show Characteristics of Active and Inactive Kinases. At the junction of the larger C-terminal lobe and the smaller N-terminal lobe resides the catalytic cleft, which contains the binding sites for substrate and ATP. The two lobes are connected by a flexible hinge that allows kinase domains to adopt two alternative ensembles of conformations: open conformations that are indicative for inactive kinases and closed conformations that are adopted by active kinases (29, 31, 32). Many kinases, including AMPK, require activation loop phosphorylation for the conformational switch from inactive to active conformation. The kinase domain of SnRK2.6 adopted an open conformation that resembles that of unphosphorylated, inactive Snf1 (30). In contrast, SnRK2.3 adopted a closed conformation very similar to that found in phosphorylated, active Snf1 (29) (Fig. 2 *B* and *C*) and showed other hallmarks of active or partially active kinases (see below). Crystal structures of kinase domains typically provide snapshots within the ensemble of the different conformations that may be adopted in physiological settings (32). Because both SnRK2.3 and -2.6 share a similar level of basal activity, it is reasonable to assume that both kinases can adopt partially active conformations in their nonphosphorylated state.

Although cleft opening and closing can also be affected by crystal packing, other important features of active kinase structures include the presence of a helix αC-orchestrated network of interactions that stabilize the binding of ATP and Mg^{2+} in the catalytic cleft, as well as the conformation of a phosphate-

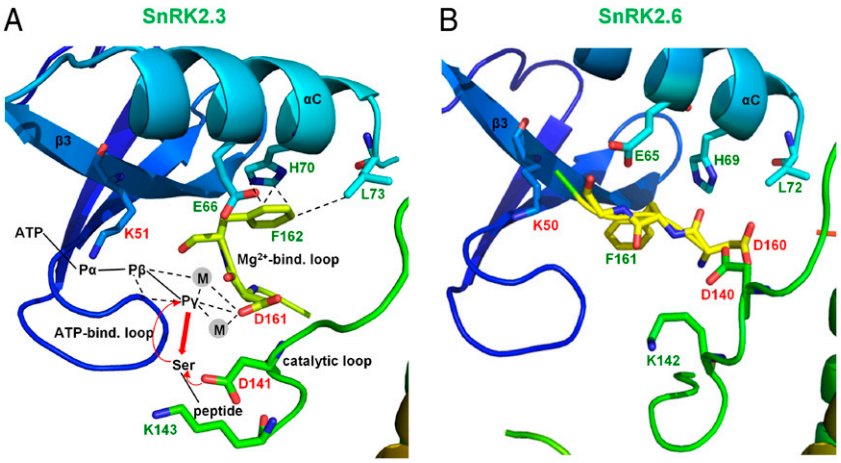

Fig. 3. Close view of the intramolecular interaction network in the SnRK2.3 and SnRK2.6 (monomer A) active sites. (*A*) SnRK2.3 adopts a partially active conformation. To illustrate active kinase features in the absence of any ATP-bound SnRK2 structure, we schematically indicated the highly conserved position of ATP with its α-, β-, and γ-phosphates (Pα, Pβ, Pγ), of the Mg^{2+}-ions (gray spheres), and the phosphate-acceptor serine based on Kornev et al. (31). The Mg^{2+}-binding DFG motif is stabilized by a hydrophobic interaction between αC and the DFG phenylalanine. ATP is positioned by three structural elements: (*i*) the ATP-binding loop (G-loop); (*ii*) the Mg^{2+}-ions complexed by the DFG aspartate; and (*iii*) by the α- and β-phosphate-binding K51, which, in turn, requires orientation by forming a salt bridge with αC E66. Note that the catalytic loop and the Mg^{2+}-binding loop adopt conserved, active positions, whereas αC E66 and K51 are at a suitable distance and on the correct side to form a salt bridge but rotated away from each other. (*B*) SnRK2.6 adopts an inactive conformation in which the K50-orienting E65, the Mg^{2+}-binding D160, and the catalytic D140 face away from the active center.

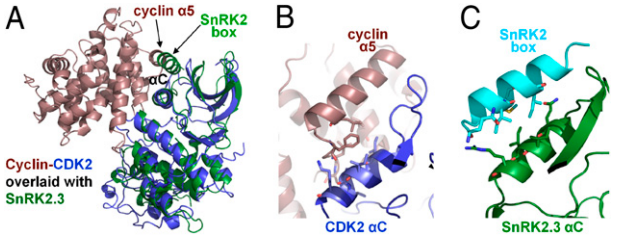

Fig. 4. The intramolecular interaction between the SnRK2 box and SnRK2.3 αC-helices mimics the intermolecular CDK2 αC stabilization by cyclin α5. (*A*) Overlay of SnRK2.3 (green) with CDK2 (blue)/cyclin A (brown). Details of the CDK2 αC–α5 (*B*) and SnRK2.3 αC–SnRK2 box (*C*) interactions. Both *B* and *C* show the same perspective from whole molecule structure alignments.

acceptor-binding aspartate in the catalytic loop (31, 33, 34). In the closed conformation of SnRK2.3, the catalytic loop and the Mg^{2+}-binding loop adopted the highly conserved conformations found in active kinases (Fig. 3*A*). The ATP-binding K51 and the K51-stabilizing residue E66 have their side chains rotated away from each other, yet sterically unconstrained rotations around two C–C single bonds are sufficient to correctly align these residues upon ATP/Mg^{2+} binding (Fig. 3*A*), suggesting a partially active state, which presents a structural rationale for the basal activity of SnRK2s. In contrast, in the open conformational snapshot of SnRK2.6, E65 is positioned too far away from the ATP-binding K50 for a productive interaction and the Mg^{2+}-binding loop is misfolded with the Mg^{2+}-binding D160 facing away from the ATP-binding site (Fig. 3*B* and *SI Appendix*, Fig. S6*B*). Taken together, our crystal structures illustrate that unphosphorylated SnRK2s can adopt conformational characteristics of both inactive and active kinases in agreement with the basal activities that we observed in our functional assays (Fig. 1). Full activation of SnRK2.3 and -2.6, similar to other Ser/Thr kinases (34), would require the closed conformation of the αC-helix and phosphorylation of the activation loop to permit full alignment of catalytic residues in the active conformation.

SnRK2 Box Stabilizes the Regulatory αC-Helix. How do SnRK2s achieve formation of partially active conformations in the absence of activation loop phosphorylation? Cleft closing and the alignment of catalytic residues is often determined by the position of the αC-helix, which, in many kinases, is modulated by the binding of regulatory proteins to the kinase domain (e.g., 34, 35, 36–41). The SnRK2 box is positioned roughly parallel to the αC-helix and makes extensive contacts with this helix to stabilize its conformation (*SI Appendix*, Fig. S8). This suggests that the SnRK2 box–αC interaction is important for kinase activity, which we tested by introducing mutations into key interaction residues. Single-point mutations that change interacting residues in the SnRK2 box (SnRK2.3 I313A, I309R, Q304A; SnRK2.6 I312A, I308R) or the αC-helix (SnRK2.3 R71A, I68R, I67R; SnRK2.6 I66R) nearly abolished kinase activity, supporting an essential role of the SnRK2 box in αC positioning (*SI Appendix*, Fig. S8, panels on the right). SnRK2.6 is noticeably less sensitive to several SnRK2 box mutations than SnRK2.3, consistent with its higher level of activation loop autophosphorylation, which is known to help stabilize the active kinase conformation (34).

Outside of the AMPK family, the SnRK2 kinase domain shows greatest homology with cyclin-dependent kinase (Cdk)2. Apo Cdk2 is completely inactive and becomes partially active upon cyclin binding, which rearranges the Cdk2 αC-helix to move toward the catalytic cleft (33, 35). This conformational change correctly aligns key residues for ATP- and Mg^{2+}-binding and enables activation loop phosphorylation to complete reorganization of the catalytic cleft to gain full activity (33, 35). As shown in Fig. 4, the intramolecular SnRK2 box–αC interaction structurally mimics the intermolecular stabilization of the Cdk2 αC helix by the cyclin α5-helix. As in the case of Cdk2/cyclin A (33, 35), the SnRK2 box–αC interaction is required for basal activity, because mutations designed to disrupt this interaction inactivate the kinase (Fig. 4). Therefore, the essential function of the SnRK2 box (5) appears to be the stabilization of αC, which is required for correct folding of the catalytic center and kinase activation, in a way that functionally resembles cyclins.

Although the SnRK2 box lacks sequence homology with cyclin α5, it shows clear homology with the α2-helix of the three-helical autoinhibitory domain (AID) of AMPK and the closely related ubiquitin-associated (UBA) domain of AMPK-related kinases (36) (*SI Appendix*, Fig. S1). Despite their sequence similarity, these domains differ in both their binding modes and regulatory functions. As shown in *SI Appendix*, Fig. S9, the AMPK AID packs against the backside of the catalytic cleft to keep the cleft in a wide open, inactive conformation (29). In contrast, the MARK UBA domain binds to the N-terminal lobe and was speculated to stabilize both inactive and active conformations

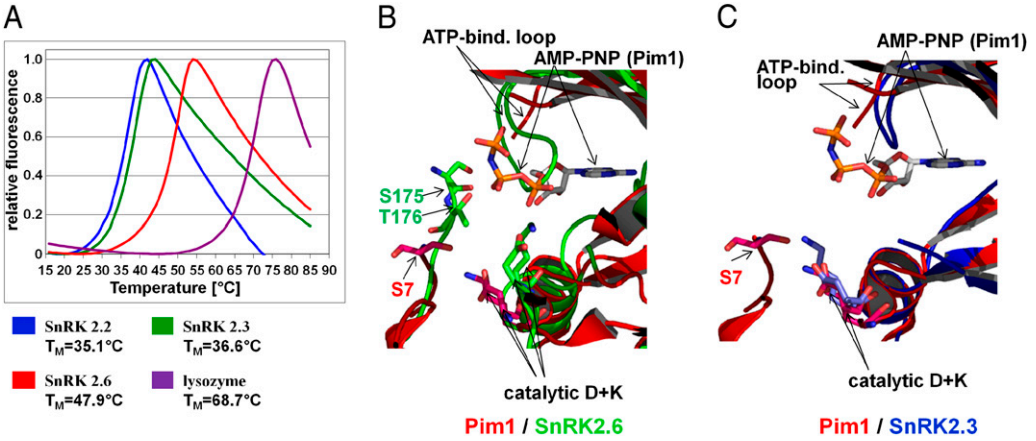

Fig. 5. SnRK2.6 is more stable than SnRK2.3 and has its phosphate-acceptor residues positioned at the catalytic site. (*A*) Melting curves of SnRK2.2, 2.3 and 2.6 with calculated T_M values. As reference, the melting curve of lysozyme is shown as well. (*B*) Overlay of the catalytic centers of SnRK2.6 (green) and Pim-1 (red), bound to a substrate peptide and the nonhydrolyzable ATP analog AMP-PNP (PDB code 2BZK). Shown as stick models are the phosphate-acceptor residues S175 and T176 (SnRK2.6 monomer B) and S7 (Pim-1 substrate peptide), AMP-PNP, and the catalytic aspartate and arginine residues from both kinases. Note that the Pim-1 ATP-binding loop is not completely resolved. (*C*) Overlay of SnRK2.3 (blue) and Pim-1, using the same orientation and crop as in (*B*).

(36), which would resemble the αC stabilization by the SnRK2 box seen in the SnRK2.3 and -2.6 structures.

SnRK2.6 Activation Loop Phosphate-Acceptor Residues Are in Close Proximity to the Catalytic Center. In the SnRK2.6 structure, part of the activation loop, including the autophosphorylated residues S175 and T176, were visible (*SI Appendix*, Fig. S6*A*). In contrast, they were not visible in the SnRK2.3 structure. Thermoshift assays also revealed that SnRK2.6 is a much more stable protein than SnRK2.2 and 2.3 (Fig. 5*A*). Together, these results suggest that the activation loop of SnRK2.6 is more stable than that of SnRK2.3 and -2.2, a possible explanation for the much higher level of autophosphorylation in SnRK2.6 (Fig. 1). To gain further insight into the mechanism of autophosphorylation, we overlaid the SnRK2.6 catalytic cleft with the structure of Pim-1, which, like the SnRK2s, is a member of the calmodulin-dependent protein kinase-related (CAMK) kinase family. The Pim-1 structure is in active conformation with a bound substrate peptide and the ATP analog AMP-PNP (42). As shown in Fig. 5*B*, SnRK2.6 S175 and T176 assume positions very close to that of the phosphorylated serine (S7) in the Pim-1 substrate peptide. Whereas the position of AMP-PNP clashes with the position of the flexible SnRK2.6 ATP-binding loop in the open conformation (Fig. 5*B*), there are no clashes in the closed conformation seen in the SnRK2.3 structure (Fig. 5*C*). Equilibrium between these conformations is, therefore, likely to rearrange this loop to allow ATP-binding and activation loop autophosphorylation of SnRK2.6. The correct positions of SnRK2.6 S175 and T176 toward the catalytic center thus provide a basis for the efficient autophosphorylation of SnRK2.6, which would then lead to its full activation, as we observed in solution (Fig. 1).

Discussion

Autoactivation of the SnRK2 kinases, triggered by receptor-mediated inhibition of PP2C, is at the center of the ABA signaling network. The structures and biochemical studies presented here help to establish a mechanism for autoactivation of SnRK2 kinases and to complete a structural framework for understanding how ABA signaling is transmitted from hormone perception by the PYR/PYL receptors to inhibition of PP2Cs and to autoactivation of the downstream effectors: SnRK2 kinases.

After completion of this work, Yunta et al. reported the crystal structures of two catalytically inactive mutants (D160A and D160A/S175A) of SnRK2.6 (43). Despite the mutations and different space groups, these structures were, as expected, in similar open, inactive conformations as the SnRK2.6 structure reported here (*SI Appendix*, Fig. S6*B*; relative to molecule A in the asymmetric unit, the root mean square deviation for molecule B is 0.817 Å, for the two molecule of the D160A mutant 0.87 and 0.76 Å, and for the two molecules of the D160A/S175A mutant 0.86 and 0.79 Å). In contrast, both SnRK2.3 and -2.6 used in our crystallization studies are fully active kinases, and our structures illustrate that the kinases can adopt either close or open conformations.

The extensive structural and biochemical data presented here illustrate a two-step activation mechanism of SnRK2 kinases. The first step is the ABA-mediated conversion of SnRK2 kinase from a PP2C-inhibited state to a partially active state, which is then further converted into a fully active state by activation loop phosphorylation. In both SnRK2.3 and -2.6 structures, the conserved SnRK2 box adopts a helical structure that forms extensive interactions with αC, which we showed is important for kinase activity. This intramolecular stabilization of αC is both structurally and functionally analogous to the intermolecular αC interaction seen in cyclin-dependent kinases, which are related to the AMPK family of kinases. However, another variation of αC displacement occurs in the tyrosine kinase Src, where an intramolecular interaction stabilizes an inactive αC conformation and disruption of that interaction allows αC to adopt a position very similar to that of SnRK2.3 and cyclin-bound Cdk2 (41). Full activation of the kinases requires phosphorylation of the activation loop, which SnRK2.6 can efficiently achieve on its own. We suggest that this is attributable to the higher stability of SnRK2.6 and the well-structured S175 and T176 residues from the activation loop, which are in close proximity to the active site. Autophosphorylation of recombinant SnRK2.2 and -2.3, which are less stable, is ∼5–10 times less efficient than for SnRK2.6, suggesting that these kinases may also be phosphorylated by as yet unknown upstream kinases, as has been suggested for several members of the SnRK2 family (6, 44). The mechanism of SnRK2 kinase activation by the SnRK2 box and phosphorylation of the activation loop resemble that of AMP-activated kinase and cyclin-dependent kinase, thus further unifying the conserved mechanism of kinase activation despite their diverse cellular functions.

Materials and Methods

Protein Preparation. WT and mutant SnRK2s were expressed in *Escherichia coli* BL21 (DE3) as H6Sumo fusion proteins and purified following the same general method as described previously for the purification of PYL1 (13). For more details, see *SI Appendix, SI Materials and Methods*.

Crystallization. SnRK2.3 D57A/K58A crystals were grown at room temperature in hanging drops containing 1 μL of the purified protein at a concentration of 15.9 mg mL^{-1} and 1 μL of well solution containing 0.2 M ammonium sulfate, 0.1 M sodium cacodylate trihydrate (pH 6.5), 25% PEG 8000, and 0.01M Hexamine cobalt (III) chloride. Crystals of ∼50–90 μm in length appeared within 2–3 d. Crystals were serially transferred to well buffer with increasing glycerol concentration [10% (vol/vol) final] before flash-freezing in liquid nitrogen.

SnRK2.6 D59A/E60A crystals were grown at room temperature in sitting drops containing 0.2 μL of the purified protein at a concentration of 6.75 mg mL^{-1} and 0.2 μL of well solution containing 5% Tacsimate (Hampton Research) (pH 7.0) and 27% PEG 3350. Crystals appeared within 1–2 d and grew to a dimension of ∼50 μm in length over a period of 10 d. Crystals were soaked in well solution with a final concentration of 40% PEG 3350 before flash-freezing in liquid nitrogen.

Data Collection and Structure Determination. All diffraction datasets were collected at 100 K using an X-ray beam at 0.97872 Å wavelength with Rayomics300 or Rayomics225 (Rayonix, Inc) CCD detectors at the ID-D and ID-F beam lines of sector 21 [Life Sciences Collaborative Access Team (LS-CAT)] at the Advanced Photon Source at Argonne National Laboratory. The observed reflections were reduced, merged, and scaled with DENZO and SCALEPACK in the HKL2000 package (45). The structure of SnRK2.3 was solved by molecular replacement using the kinase domain of human AMPK α2 (PDB code 2H6D, with loop regions deleted) as a search model. The SnRK2.6 structure was solved by molecular replacement using SnRK2.3 as a search model. Molecular replacement was performed by using the Collaborative Computational Project 4 (CCP4) program Phaser (46). Programs O and Coot were used to manually fit the protein models (47, 48). Model refinement was performed with CNS and the CCP4 program Refmac5 (49, 50).

ACKNOWLEDGMENTS. We thank the staff of LS-CAT for assistance in data collection at the beam lines of sector 21, which is funded, in part, by the Michigan Economic Development Corporation and the Michigan Technology Tri-Corridor. Use of the Advanced Photon Source was supported by the Office of Science of the US Department of Energy. This work was supported by The Jay and Betty Van Andel Foundation and Amway (China) Limited (H.E.X.), the National Institutes of Health (H.E.X., P.R.G., and J.-K.Z.), and the Singapore Biomedical Research Council (E.-L.Y.). L.-M.N. and F.-F.S. were supported by an overseas PhD scholarship from the National University of Singapore Graduate School for Integrative Sciences and Engineering (NGS).

1. Tuteja N (2007) Abscisic Acid and abiotic stress signaling. *Plant Signal Behav* 2:135–138.
2. Fujii H, et al. (2009) In vitro reconstitution of an abscisic acid signalling pathway. *Nature* 462:660–664.
3. Umezawa T, et al. (2009) Type 2C protein phosphatases directly regulate abscisic acid-activated protein kinases in Arabidopsis. *Proc Natl Acad Sci USA* 106:17588–17593.

4. Fujii H, Zhu JK (2009) Arabidopsis mutant deficient in 3 abscisic acid-activated protein kinases reveals critical roles in growth, reproduction, and stress. *Proc Natl Acad Sci USA* 106:8380–8385.
5. Belin C, et al. (2006) Identification of features regulating OST1 kinase activity and OST1 function in guard cells. *Plant Physiol* 141:1316–1327.
6. Boudsocq M, Droillard MJ, Barbier-Brygoo H, Laurière C (2007) Different phosphorylation mechanisms are involved in the activation of sucrose non-fermenting 1 related protein kinases 2 by osmotic stresses and abscisic acid. *Plant Mol Biol* 63:491–503.
7. Cutler SR, Rodriguez PL, Finkelstein RR, Abrams SR (2010) Abscisic acid: Emergence of a core signaling network. *Annu Rev Plant Biol* 61:651–679.
8. Hubbard KE, Nishimura N, Hitomi K, Getzoff ED, Schroeder JI (2010) Early abscisic acid signal transduction mechanisms: Newly discovered components and newly emerging questions. *Genes Dev* 24:1695–1708.
9. Yin P, et al. (2009) Structural insights into the mechanism of abscisic acid signaling by PYL proteins. *Nat Struct Mol Biol* 16:1230–1236.
10. Ma Y, et al. (2009) Regulators of PP2C phosphatase activity function as abscisic acid sensors. *Science* 324:1064–1068.
11. Park SY, et al. (2009) Abscisic acid inhibits type 2C protein phosphatases via the PYR/PYL family of START proteins. *Science* 324:1068–1071.
12. Vlad F, et al. (2009) Protein phosphatases 2C regulate the activation of the Snf1-related kinase OST1 by abscisic acid in Arabidopsis. *Plant Cell* 21:3170–3184.
13. Melcher K, et al. (2009) A gate-latch-lock mechanism for hormone signalling by abscisic acid receptors. *Nature* 462:602–608.
14. Miyazono K, et al. (2009) Structural basis of abscisic acid signalling. *Nature* 462: 609–614.
15. Nishimura N, et al. (2009) Structural mechanism of abscisic acid binding and signaling by dimeric PYR1. *Science* 326:1373–1379.
16. Santiago J, et al. (2009) The abscisic acid receptor PYR1 in complex with abscisic acid. *Nature* 462:665–668.
17. Hao Q, et al. (2010) Functional mechanism of the abscisic acid agonist pyrabactin. *J Biol Chem* 285:28946–28952.
18. Melcher K, et al. (2010) Identification and mechanism of ABA receptor antagonism. *Nat Struct Mol Biol* 17:1102–1108.
19. Peterson FC, et al. (2010) Structural basis for selective activation of ABA receptors. *Nat Struct Mol Biol* 17:1109–1113.
20. Furihata T, et al. (2006) Abscisic acid-dependent multisite phosphorylation regulates the activity of a transcription activator AREB1. *Proc Natl Acad Sci USA* 103:1988–1993.
21. Johnson RR, Wagner RL, Verhey SD, Walker-Simmons MK (2002) The abscisic acid-responsive kinase PKABA1 interacts with a seed-specific abscisic acid response element-binding factor, TaABF, and phosphorylates TaABF peptide sequences. *Plant Physiol* 130:837–846.
22. Soon F.-F., et al. (2011) Molecular mimicry regulates ABA signaling by SnRK2 kinases and PP2C phosphatases. *Science*, 10.1126/science.1215106.
23. Lochhead PA (2009) Protein kinase activation loop autophosphorylation in cis: Overcoming a Catch-22 situation. *Sci Signal* 2:pe4.
24. Wang J, Wu JW, Wang ZX (2011) Mechanistic studies of the autoactivation of PAK2: A two-step model of cis initiation followed by trans amplification. *J Biol Chem* 286: 2689–2695.
25. Littler DR, et al. (2010) A conserved mechanism of autoinhibition for the AMPK kinase domain: ATP-binding site and catalytic loop refolding as a means of regulation. *Acta Crystallogr Sect F Struct Biol Cryst Commun* 66:143–151.
26. Chalmers MJ, Busby SA, Pascal BD, Southern MR, Griffin PR (2007) A two-stage differential hydrogen deuterium exchange method for the rapid characterization of protein/ligand interactions. *J Biomol Tech* 18:194–204.
27. Derewenda ZS (2004) Rational protein crystallization by mutational surface engineering. *Structure* 12:529–535.
28. Derewenda ZS, Vekilov PG (2006) Entropy and surface engineering in protein crystallization. *Acta Crystallogr D Biol Crystallogr* 62:116–124.
29. Chen L, et al. (2009) Structural insight into the autoinhibition mechanism of AMP-activated protein kinase. *Nature* 459:1146–1149.
30. Nayak V, et al. (2006) Structure and dimerization of the kinase domain from yeast Snf1, a member of the Snf1/AMPK protein family. *Structure* 14:477–485.
31. Kornev AP, Haste NM, Taylor SS, Eyck LF (2006) Surface comparison of active and inactive protein kinases identifies a conserved activation mechanism. *Proc Natl Acad Sci USA* 103:17783–17788.
32. Rabiller M, et al. (2010) Proteus in the world of proteins: Conformational changes in protein kinases. *Arch Pharm (Weinheim)* 343:193–206.
33. Pavletich NP (1999) Mechanisms of cyclin-dependent kinase regulation: Structures of Cdks, their cyclin activators, and Cip and INK4 inhibitors. *J Mol Biol* 287:821–828.
34. Nolen B, Taylor S, Ghosh G (2004) Regulation of protein kinases; controlling activity through activation segment conformation. *Mol Cell* 15:661–675.
35. Jeffrey PD, et al. (1995) Mechanism of CDK activation revealed by the structure of a cyclinA-CDK2 complex. *Nature* 376:313–320.
36. Marx A, Nugoor C, Panneerselvam S, Mandelkow E (2010) Structure and function of polarity-inducing kinase family MARK/Par-1 within the branch of AMPK/Snf1-related kinases. *FASEB J* 24:1637–1648.
37. Kannan N, Haste N, Taylor SS, Neuwald AF (2007) The hallmark of AGC kinase functional divergence is its C-terminal tail, a cis-acting regulatory module. *Proc Natl Acad Sci USA* 104:1272–1277.
38. Zhang X, Gureasko J, Shen K, Cole PA, Kuriyan J (2006) An allosteric mechanism for activation of the kinase domain of epidermal growth factor receptor. *Cell* 125: 1137–1149.
39. Lamers MB, Antson AA, Hubbard RE, Scott RK, Williams DH (1999) Structure of the protein tyrosine kinase domain of C-terminal Src kinase (CSK) in complex with staurosporine. *J Mol Biol* 285:713–725.
40. Bayliss R, Sardon T, Vernos I, Conti E (2003) Structural basis of Aurora-A activation by TPX2 at the mitotic spindle. *Mol Cell* 12:851–862.
41. Huse M, Kuriyan J (2002) The conformational plasticity of protein kinases. *Cell* 109: 275–282.
42. Bullock AN, Debreczeni J, Amos AL, Knapp S, Turk BE (2005) Structure and substrate specificity of the Pim-1 kinase. *J Biol Chem* 280:41675–41682.
43. Yunta C, Martínez-Ripoll M, Zhu JK, Albert A (2011) The structure of Arabidopsis thaliana OST1 provides insights into the kinase regulation mechanism in response to osmotic stress. *J Mol Biol* 414:135–144.
44. Burza AM, et al. (2006) Nicotiana tabacum osmotic stress-activated kinase is regulated by phosphorylation on Ser-154 and Ser-158 in the kinase activation loop. *J Biol Chem* 281:34299–34311.
45. Otwinowski Z, Borek D, Majewski W, Minor W (2003) Multiparametric scaling of diffraction intensities. *Acta Crystallogr A* 59:228–234.
46. McCoy AJ, et al. (2007) Phaser crystallographic software. *J Appl Cryst* 40:658–674.
47. Emsley P, Cowtan K (2004) Coot: Model-building tools for molecular graphics. *Acta Crystallogr D Biol Crystallogr* 60:2126–2132.
48. Kleywegt GJ, Jones TA (1996) Efficient rebuilding of protein structures. *Acta Crystallogr D Biol Crystallogr* 52:829–832.
49. Brünger AT, et al. (1998) Crystallography & NMR system: A new software suite for macromolecular structure determination. *Acta Crystallogr D Biol Crystallogr* 54: 905–921.
50. Murshudov GN, Vagin AA, Lebedev A, Wilson KS, Dodson EJ (1999) Efficient anisotropic refinement of macromolecular structures using FFT. *Acta Crystallogr D Biol Crystallogr* 55:247–255.

Structural basis for basal activity and auto-activation of ABA signaling SnRK2 kinases

Ley-Moy Ng [1,2*], Fen-Fen Soon [1,2*], X. Edward Zhou [1*], Graham M. West [3], Amanda Kovach [1], Kelly M. Suino-Powell [1], Michael J. Chalmers [3], Jun Li [1, 2], Eu-Leong Yong[2], Jian-Kang Zhu[4,5], Patrick R. Griffin [3], Karsten Melcher [1§], and H. Eric Xu [1,6§]

Supporting Information

This supplement contains:

SI Materials and Methods

Figs. S1 to S9

Table S1

SI Materials and Methods

Protein preparation. Wild type and mutant SnRK2s were expressed in *E. coli* BL21 (DE3) as H6Sumo fusion proteins and purified following the same general method as described previously for the purification of PYL1 (1). Briefly, proteins were first purified by Ni-chromatography, followed by proteolytic cleavage of the H6Sumo tag and dialysis. The cleaved H6Sumo tag was removed by re-binding to a Nickel HP column, and further purified by gel filtration chromatography (HiLoad 26/60 Superdex 200) in 25 mM Tris, pH8.0, 200 mM ammonium acetate, 1 mM dithiotreitol and 1 mM EDTA. HAB1 was purified as described (1). We generated a total of 10 sets of SnRK2.3 (D41A/K41A, E46A, D57A/K58A, D60A/E61A, R191A/Q192A/E193A, K197A, E222A/E223A, R225A, K280A, E298A) and 11 sets of SnRK2.6 (D40A/K41A, E45A, E56A/K57A, D59A/E60A, K190A/K191A/E192A, K196A, E221A/E222A, K224A, K264A, K279A, D296A/E297A) surface entropy mutants. Mutated residues were predicted to be solvent-exposed and within flexible loops based on the position of the homologous amino acids in the Snf1 structure. All mutant proteins were catalytically active and interacted with HAB1, but only SnRK2.3 D57A/K58A and SnRK2.6 D59A/E60A yielded diffraction quality crystals.

Hydrogen/Deuterium Exchange and Mass Spectrometry. Solution phase HDX experiments were performed with a LEAP Technologies Twin HTS PAL liquid handling robot interfaced with an Orbitrap mass spectrometer (Exactive, ThermoFisher Scientific) (2). SnRK2 solutions were prepared at 15 µM by diluting stocks detailed in the Proteins Preparation section above into a buffer consisting of 25 mM Tris HCl, 200 mM ammonium acetate, 1 mM EDTA, 1 mM DTT at pH 8.0. These 15 μM solutions were diluted 1:4 into the same buffer dissolved in D_2O buffer (or H_2O buffer for “0 second” samples) and incubated for predetermined times (10, 30, 60, 300, 900 and 3600 seconds) at 4°C before quenching. Quenching was performed by combining 20 μL of incubating kinase solution with 30 μL of 3 M Urea in 1.0% TFA at 1°C. Digestion was performed in line with chromatography using an in-house packed pepsin column (3) at 50 µl/min and peptides were captured and desalted on a 2 mm i.d. C8 trap (Thermo Fisher Scientific, San Jose, CA). Peptides were then separated across a 10x1 mm (5µm) Hypersil Gold C8 column (Thermo Fisher Scientific, San Jose, CA) with a linear gradient of 12-40% acetonitrile in 0.3% formic acid over five minutes. Peptide ion signals were confirmed if they had a MASCOT score of 20 or greater and had no ambiguous hits using a decoy (reverse) sequence in a separate experiment using a 60 minute gradient. The intensity weighted average m/z value (centroid) of each peptide’s isotopic envelope was calculated with the in-house developed software HD Desktop (4) and corrected for back-exchange.

To determine the phosphorylation status of SnRK2s, peptides corresponding to phosphorylated and unphosphorylated ion signals were sequenced in separate MS/MS experiments. Kinases in these MS/MS experiments were incubated in the presence and absence of ATP (1 hour ATP incubation). All samples, for both MS/MS experiments and MS experiments, contained 10 μM kinase, 10 mM Mg^{2+}, and 0.2 mM ATP. HAB1 was at 10 μM when present. Ratios of phosphorylated to unphosphorylated peptide were calculated from area under the curve measurements of monoisotopic ion signals.

Kinase Assays. SnRK2 kinases were either pre-incubated with HAB1 in kinase buffer (25 mM Tris, pH 7.4, 12 mM $MgCl_2$, 2 mM DTT) for 30 minutes at room temperature or were directly incubated with 0.2 mM unlabelled ATP, 2.5 µCi [^{32}P]-γATP, and 2 µM GST-ABF2(73-120) for 30 min (or the indicated amount of time in Fig. 1A) at room temperature in a total volume of 15 µl. Reactions were terminated by addition of SDS sample buffer and subjected to Tricine SDS-PAGE. Gels were stained with Coomassie and subjected to autoradiography using a FLA-5000 phosphor imager (Fuji).

AlphaScreen assays. Interactions between SnRK2s and HAB1 were assessed by luminescence-proximity AlphaScreen technology as described previously (1). Reactions contained 100 nM recombinant H6GST-SnRK2.6 proteins bound to nickel-acceptor beads and 100 nM recombinant biotin-HAB1 bound to streptavidin donor beads.

Mutagenesis. Site-directed mutagenesis was carried out using the QuikChange method (Agilent). Mutations and all plasmid constructs were confirmed by sequencing.

Thermoshift assay. Reactions were set up in final volumes of 10 µl in 96-well plates with 10x SYPRO Orange (Invitrogen), using the StepOnePlus™ Real-Time PCR System (Applied Biosystems) melt curve program with a ramp rate of 1 ˚C and temperature range of 15 ˚C to 85 ˚C.

Supplemental References

1. Melcher, K., Ng, L. M., Zhou, X. E., Soon, F. F., Xu, Y*., et al.* (2009) A gate-latch-lock mechanism for hormone signalling by abscisic acid receptors. *Nature* 462: 602-608.
2. Chalmers, M. J., Busby, S. A., Pascal, B. D., He, Y., Hendrickson, C. L*., et al.* (2006) Probing protein ligand interactions by automated hydrogen/deuterium exchange mass spectrometry. *Anal. Chem.* 78: 1005-1014.
3. Busby, S. A., Chalmers, M. J., & Griffin, P. R. (2007) Improving digestion efficiency under H/D exchange conditions with activated pepsinogen coupled columns. *Int. J. Mass Spect.* 259: 130-139.
4. Pascal, B. D., Chalmers, M. J., Busby, S. A., & Griffin, P. R. (2009) HD desktop: an integrated platform for the analysis and visualization of H/D exchange data. *J. Am. Soc. Mass Spectrom.* 20: 601-610.

Supplemental Table 1:

Statistics of data sets and structure refinement

	SnRK2.3	**SnRK2.6**
PDB code	3UC3	3UC4
Data collection		
APS beam line	21-ID-F	21-ID-D
Space group	$P3_121$	$C222_1$
Resolution, Å	30-1.90	30-2.30
Cell parameters, Å, °	a=75.41, b=75.41, c=116.434; α=β=90, γ=120	a=76.11, b=171.54, c=116.24;α=β=γ=90
Total/Unique reflections	209703 /30806	216364/34851
Completeness, %	100.0 (100.0)	100.0 (100.0)
I/σ	20.77 (3.3)	19.7 (2.9)
Redundancy	6.8 (6.8)	6.2 (6.3)
R_{sym}	0.079 (0.594)	0.086 (0.653)
Structure Determination		
Resolution, Å	30-1.90	30-2.30
No. reflections	28568	31695
Molecules per A.U.	1	2
No. residues	271	574
No. solvent molecules	143	115
No. of non-H atoms	2332	4726
R_{cryst}	21.2%	22.0%
R_{free}	22.9%	24.6%
rmsd bonds, Å	0.008	0.012
rmsd angles, °	1.065	1.171
Average B factor, $Å^2$	25.69	40.11

Supplemental Fig. 1

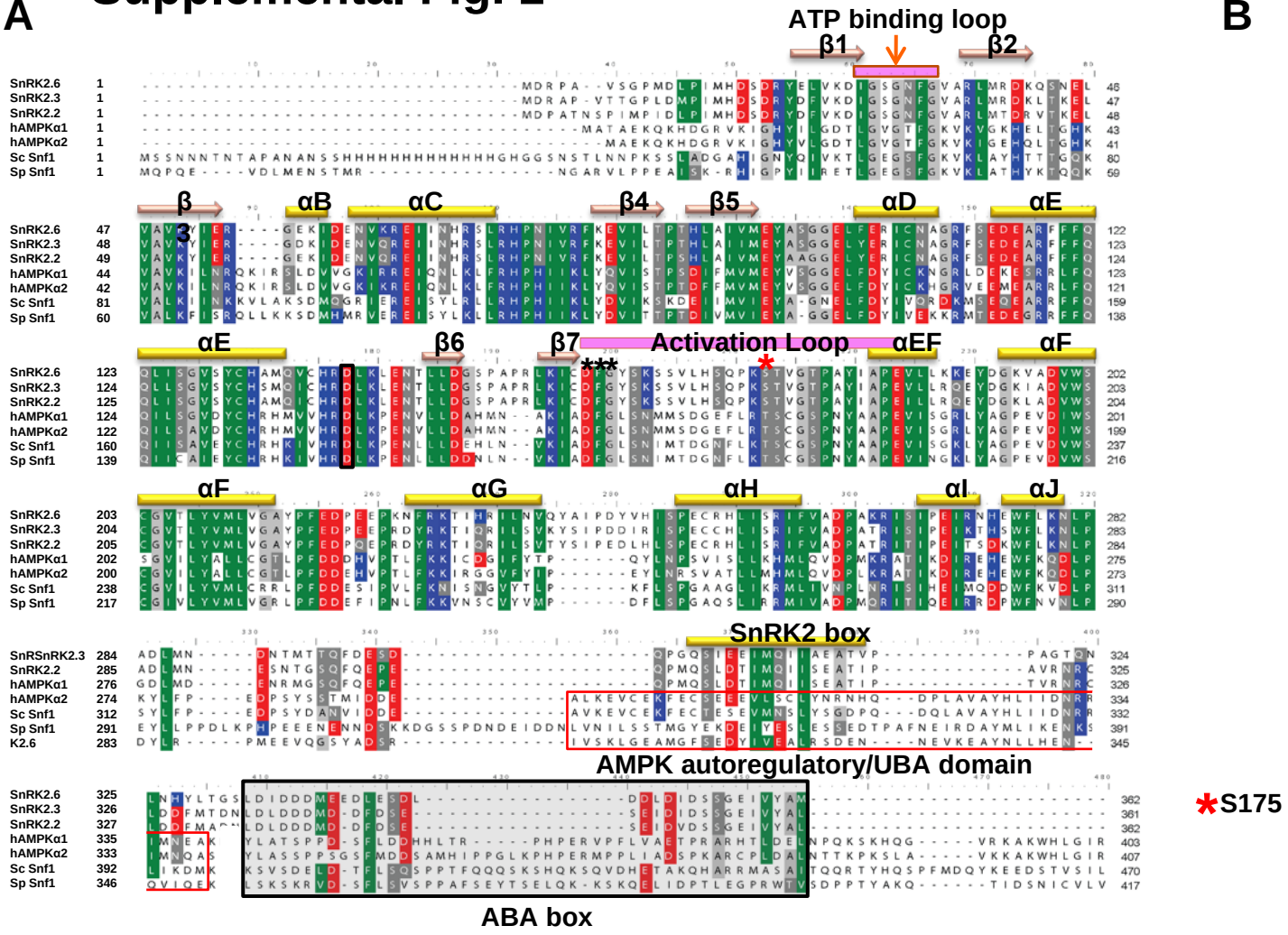

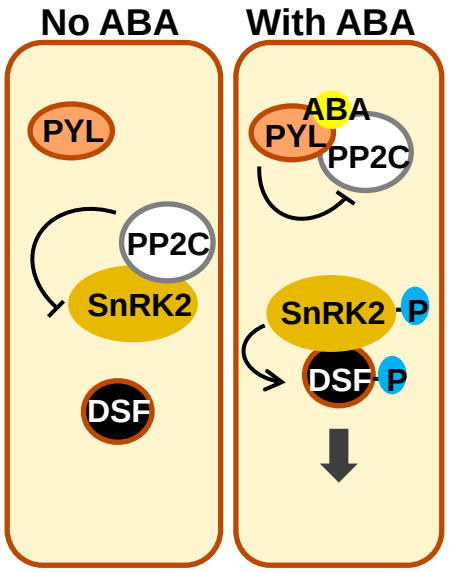

*S175

Supplemental Figure 1: SnRK2 sequence and model of SnRK2/ABA signaling. (*A*) Structure-based sequence alignment of the three SnRK2s with the α1 and α2 subunits of human AMPK and *S. cerevisiae* and *S. pombe* Snf1. Secondary structure elements and the ATP binding loop, activation loop, SnRK2 box, AMPK autoregulatory/UBA domain (red box), and ABA box (shaded rectangle) are indicated. The conserved DFG motif of the Mg^{2+}-binding loop is indicated by asterisks. The alignment was performed using BioEdit, with the program ClustalW and the similarity matrix BLOSUM62 using default parameters. (*B*) Cartoon presentation (modified from 11) of the core ABA signaling pathway. In the absence of ABA, the SnRK2 kinases are inhibited by PP2Cs. In the presence of ABA, the PYL ABA receptors form a complex with ABA and PP2Cs that inhibits PP2C catalytic activity, allowing SnRK2 autoactivation and phosphorylation of downstream factors (DSFs).

Supplemental Fig. 2

A

SnRK2.6		SnRK2.6 + HAB		SnRK2.3		SnRK2.2	
sequence	**z**	**sequence**	**z**	**sequence**	**z**	**sequence**	**z**
S7: GSMDRPAV**S**GPM	1					**S7:** GSMDPATNSPIMPIDL	2
S7: GSMDRPAV**S**GPM	2						
S7: GSMDRPAV**S**GPMDL	2						
S7: GSMDRPAV**S**GPMDL PIMHDSDRYELVKDI GSGNFGVARL	3						
S29: LVKDIG**S**GNFGVARL	2					**S31:** FVKDIG**S**GNFGVARL	2
S29: VKDIG**S**GNFGVARL	2	**S29:** VKDIG**S**GNFGVAR	2	**S30:** VKDIG**S**GNFGVARL	2	**S31:** VKDIG**S**GNFGVARL	2
S175/T176: HSQPK**ST**VGTPAYIA PEVL	2						
S175/T176: HSQPK**ST**VGTPAYIA PEVLLKKEYDGKVAD VWSCGVTL	4						
				S203: LRQEYDGKIADVW**S**CG	2		

B

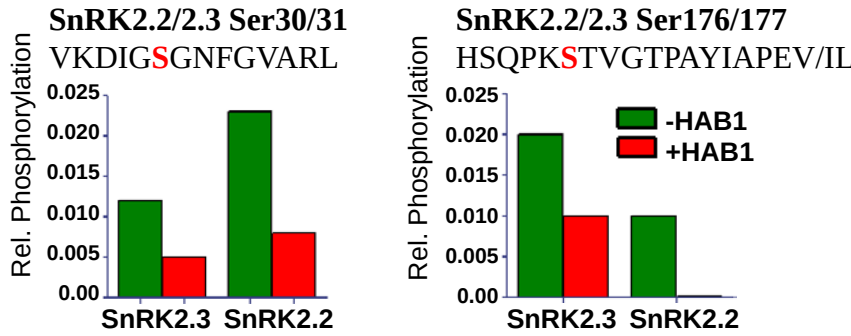

C

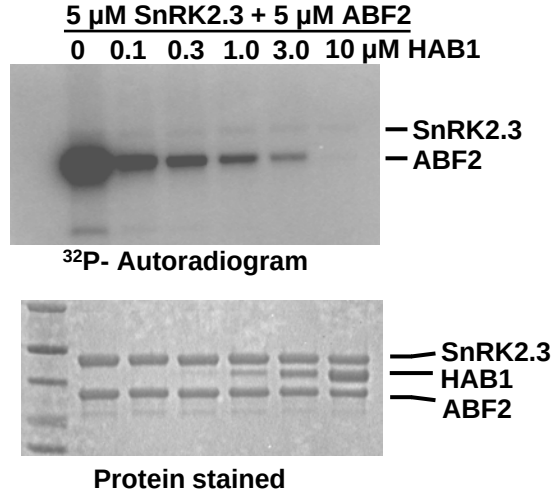

Supplemental Figure 2: Activation loop phosphorylation of recombinant SnRK2s in the presence and absence of HAB1. (A) Determination of phosphorylation sites in SnRK2s by mass spectrometry. Sequences of peptides with phosphorylated residues identified by mass spectrometry. Peptide coverage SnRK2.2: 93%, 2.3: 96%, 2.6: 68%, 2.6+HAB1: 79%. (*B*) Comparison of the ratio of phosphorylated and unphosphorylated peptides from N-terminus (/30/31) and activation loop (/176/177) of SnRK2 kinases in the presence of ATP and the presence and absence of HAB1 (see Methods). For comparison, the ratio for SnRK2.6 Ser 29 is 3 (without HAB1) and 1.5 (with HAB1) and for activation loop Ser 175 is 3 (without HAB1) and 0.03 (with HAB1) (22). (*C*) Inhibition of SnRK2.3 activity by HAB1. Increasing amounts of HAB1 were added to a kinase reaction with 5 µM SnRK2.3 and 1 µM ABF2. At high HAB1 concentrations, SnRK2.3 activity is completely inhibited. Similar inhibition has been seen for SnRK2.6 (22).

Supplemental Fig. 3

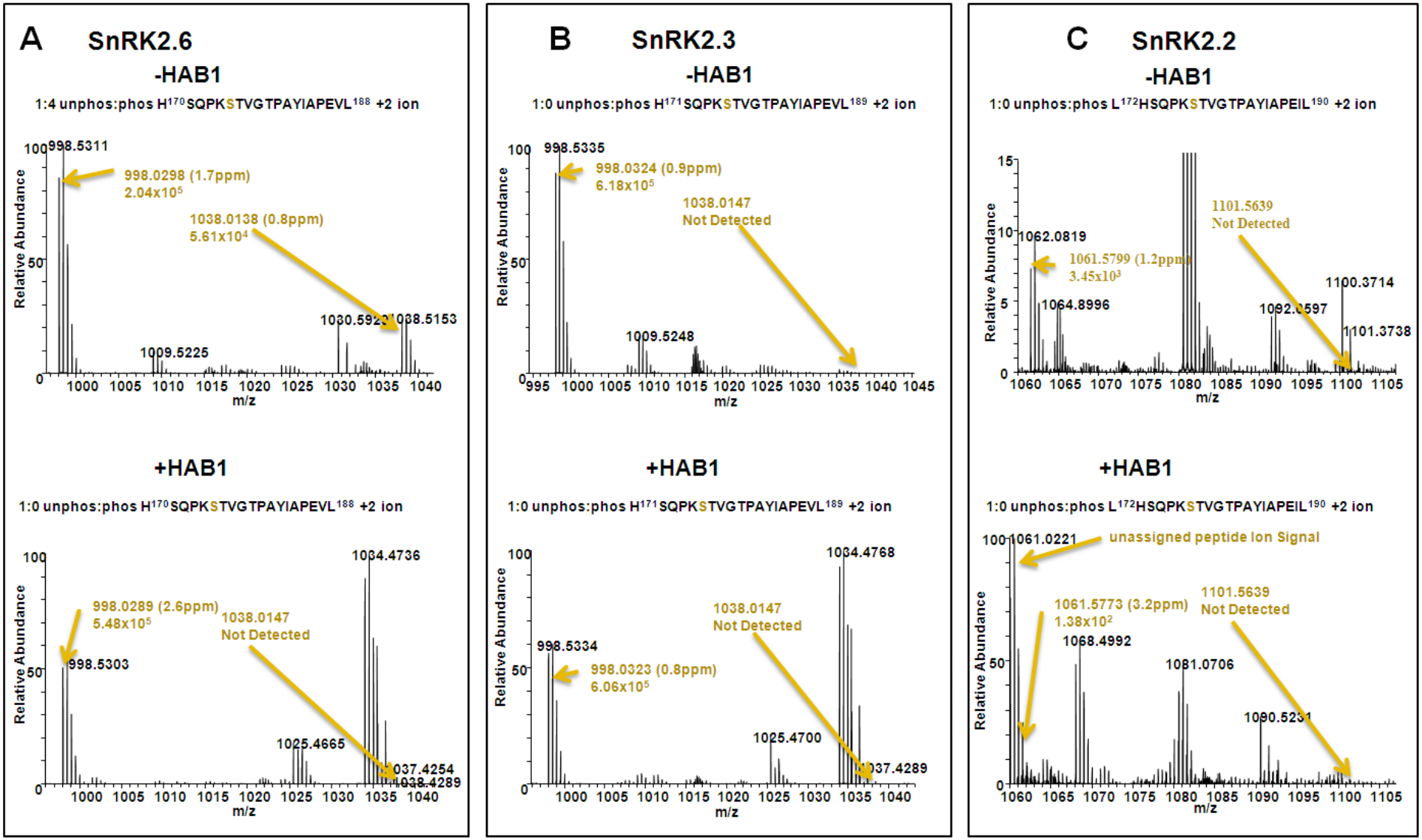

Supplemental Figure 3: Activation loop phosphorylation of recombinant SnRK2s in the presence and absence of HAB1. (*A-C*) Relative S175 (SnRK2.6) (*A*), S176 (SnRK2.3) (*B*), and S177 (SnRK2.2) (*C*) phosphorylation levels were measured by mass spectrometry based on relative ion signals intensities. The mass spectra shown have been selected from control samples in HDX experiment that did not contain D_2O. No ATP was present in these samples. The ion signal intensities are listed below the masses when detected. Arrows mark the monoisotopic ion signals of unphosphorylated and phosphorylated activation loop peptides within 5 ppm of the theoretical m/z. Top: Mass spectra of SnRK2 peptides in the absence of HAB1. Bottom: Mass spectra of SnRK2 peptides in the presence of HAB1.

Supplemental Fig. 4

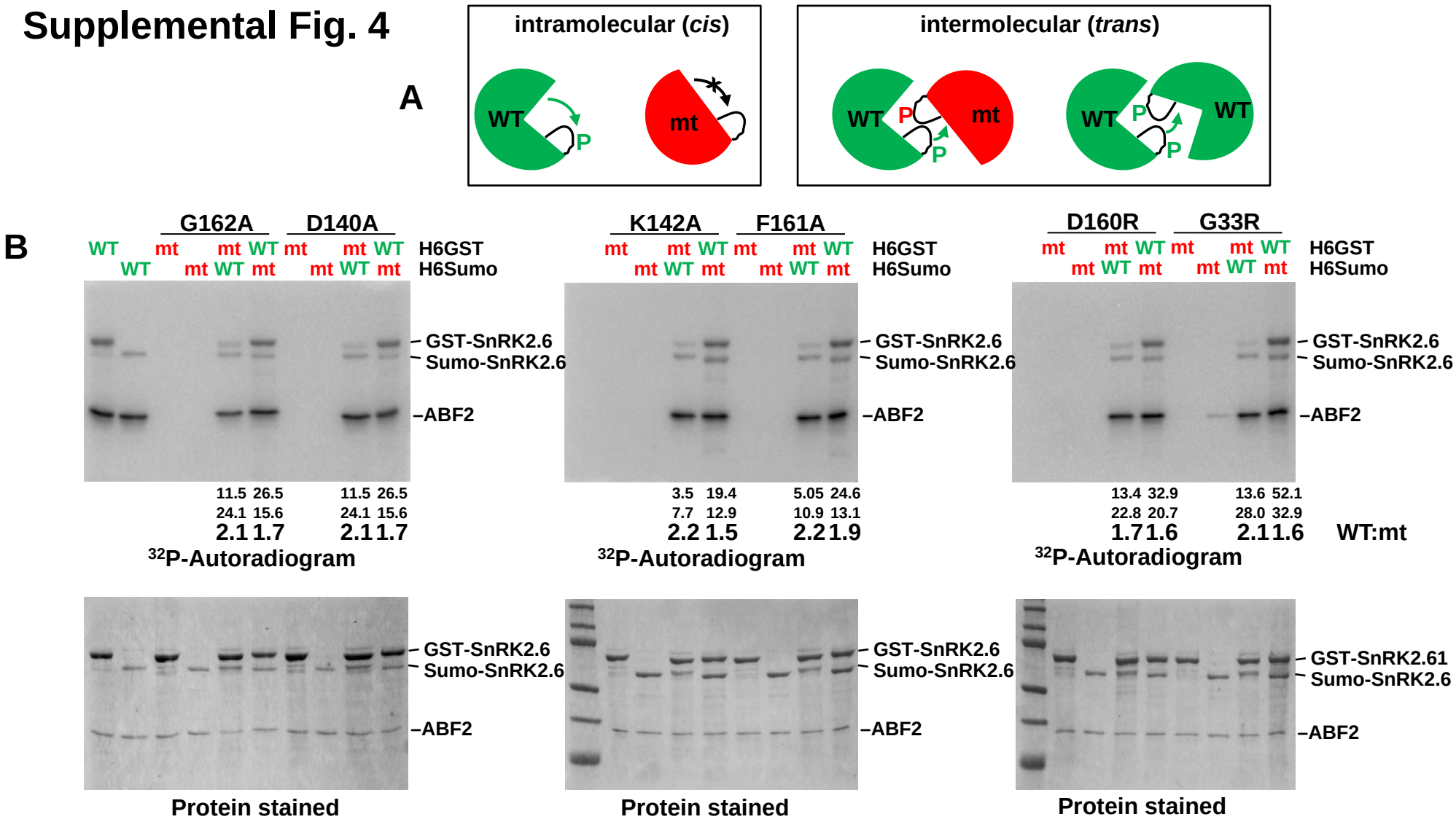

Supplemental Figure 4: SnRK2.6 *trans* and *cis* autophosphorylation. (*A*) Cartoon outlines of the experimental design and expected results to distinguish *trans* and *cis* phosphorylation of SnRK2.6 kinase. *Cis* autophosphorylation would cause [^{32}P]-phosphate incorporation into wildtype SnRK2.6 only, while *trans* autophosphorylation would cause equal incorporation into wildtype and mutant SnRK2.6. (*B*) Kinase reactions employing wildtype and mutant SnRK2.6 fused to either the larger H6GST tag (GST-SnRK2.6) or the smaller H6Sumo tag (Sumo-SnRK2.6). Note that with the exception of the naturally occurring SnRK2.6 G33R mutant none of the SnRK2.6 mutants displayed kinase activity under these reaction conditions. Numbers below autoradiogram: densitometry of H6GST-SnRK2.6 and H6Sumo-SnRK2.6, normalized to the amount of proteins loaded, and the ratios of normalized wildtype (WT) to mutant (mt) phosphorylation bands.

Supplemental Fig. 5

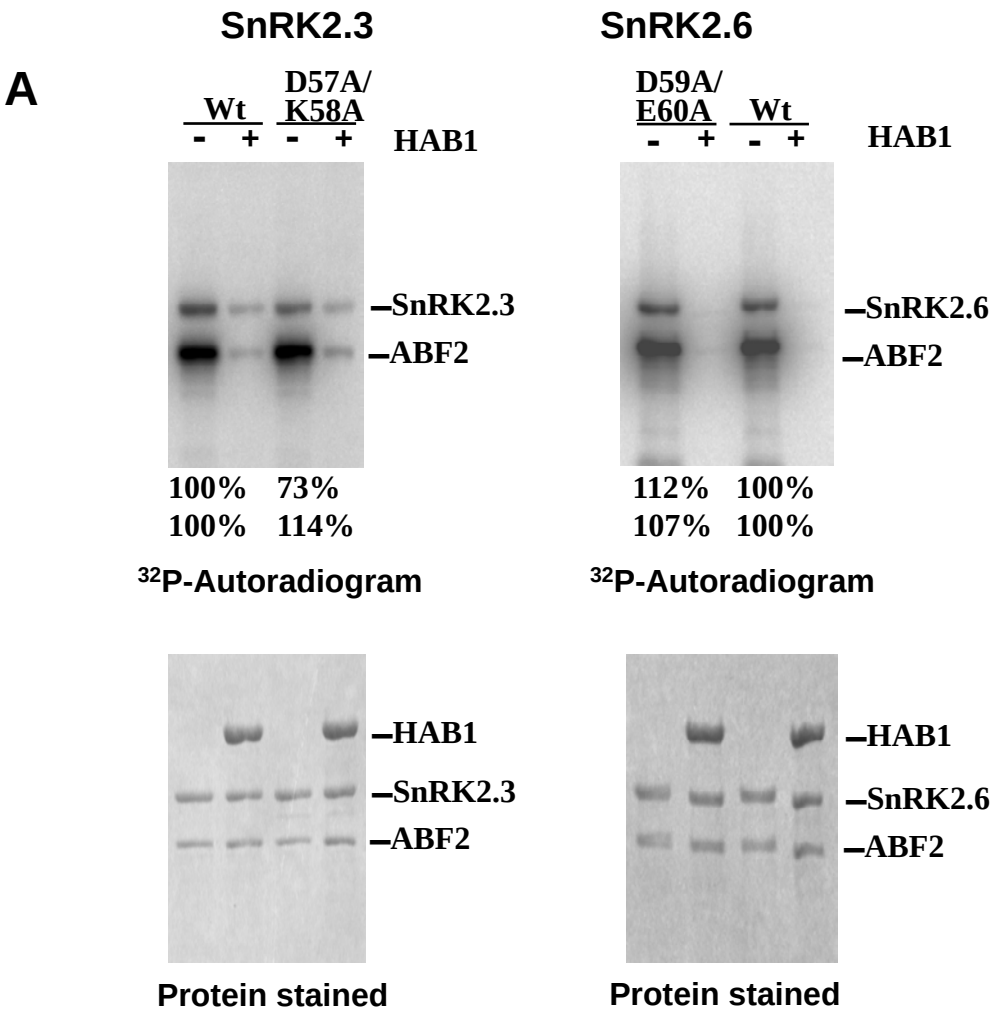

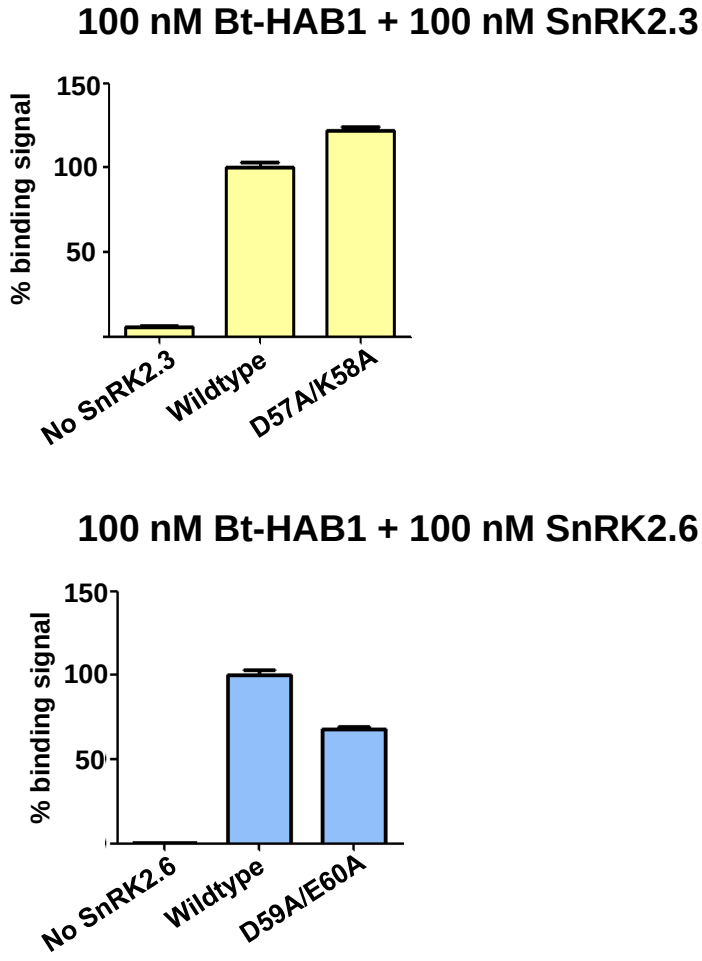

Supplemental Figure 5: SnRK2 surface entropy reduction mutant proteins are active. (*A*) Kinase assays of SnRK2.3 and 2.6 wildtype and mutant proteins in the absence and presence of HAB1. Shown are the results for the two mutants that have yielded crystal structures: E56A/K57A (apo SnRK2.3) and D59A/E60A (apo SnRK2.6). Numbers below autoradiogram: densitometry of autophosphorylation (top) and ABF2 (bottom) phosphorylation bands relative to wildtype. (*B*) AlphaScreen luminescence proximity interaction assays between biotinylated MBP-HAB1 (Bt -HAB1) and wildtype and mutant H6GST-SnRK2.3 and -2.6 proteins. Error bars indicate SD (n = 3).

Supplemental Fig. 6

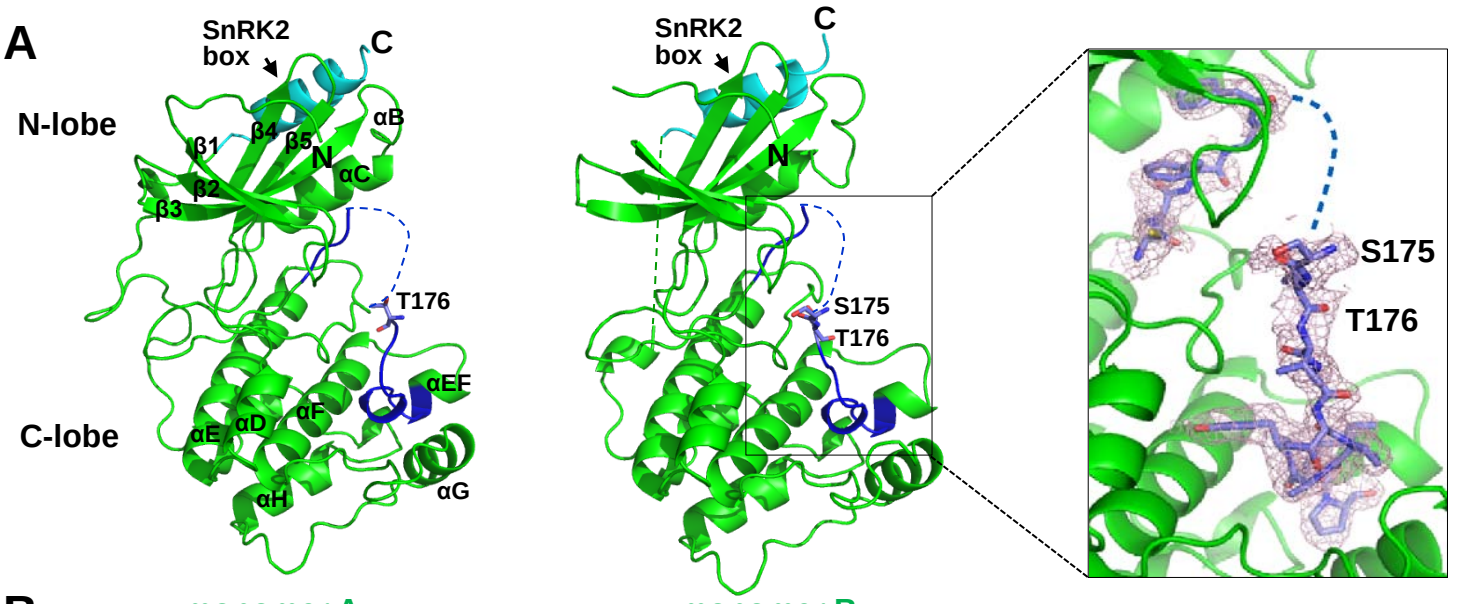

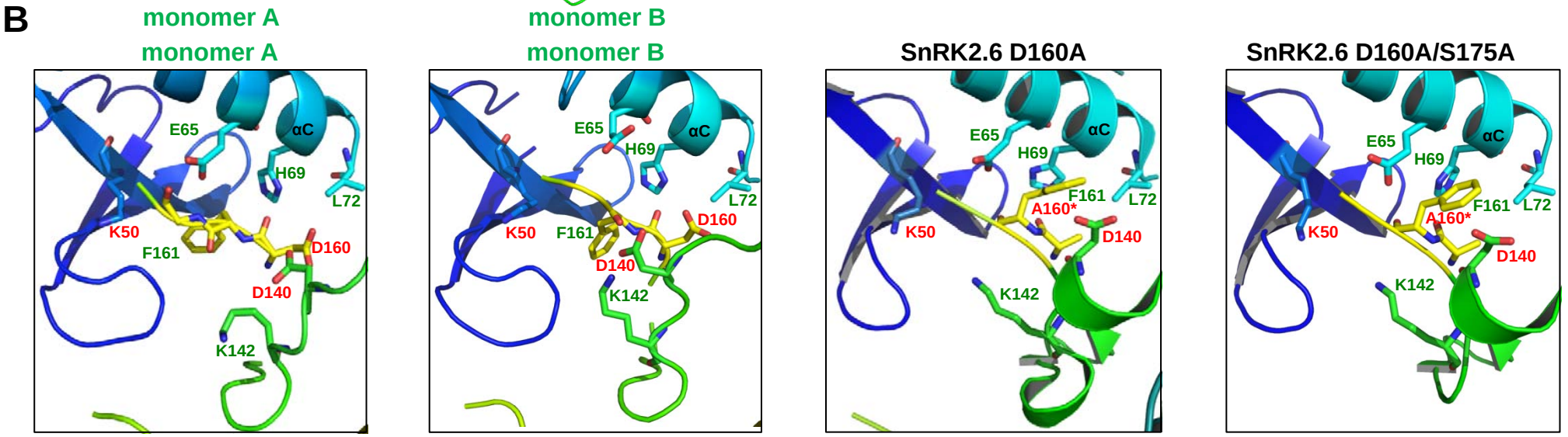

Supplemental Figure 6: SnRK2.6 structure comparison. (*A*) Structures of the two SnRK2.6 monomers found in the SnRK2.6 asymmetric unit . Ser175 and Thr176 from the activation loop are shown in stick presentation, parts of SnRK2.6 not resolved in the structures are indicated as dashed lines. The activation loop area of monomer B is shown as detail with $2F_o$-F_c composite omit map of the activation loop contoured at 1σ. (*B*) Side-by-side views of the reaction centers of the two SnRK2.6 monomers from the asymmetric unit and of the two catalytically inactive mutants (D160A mutation marked by an asterisk) described in (42). The asymmetric units of the two mutant proteins contained one more monomer, each, with all monomers being very similar to each other (43).

Supplemental Fig. 7

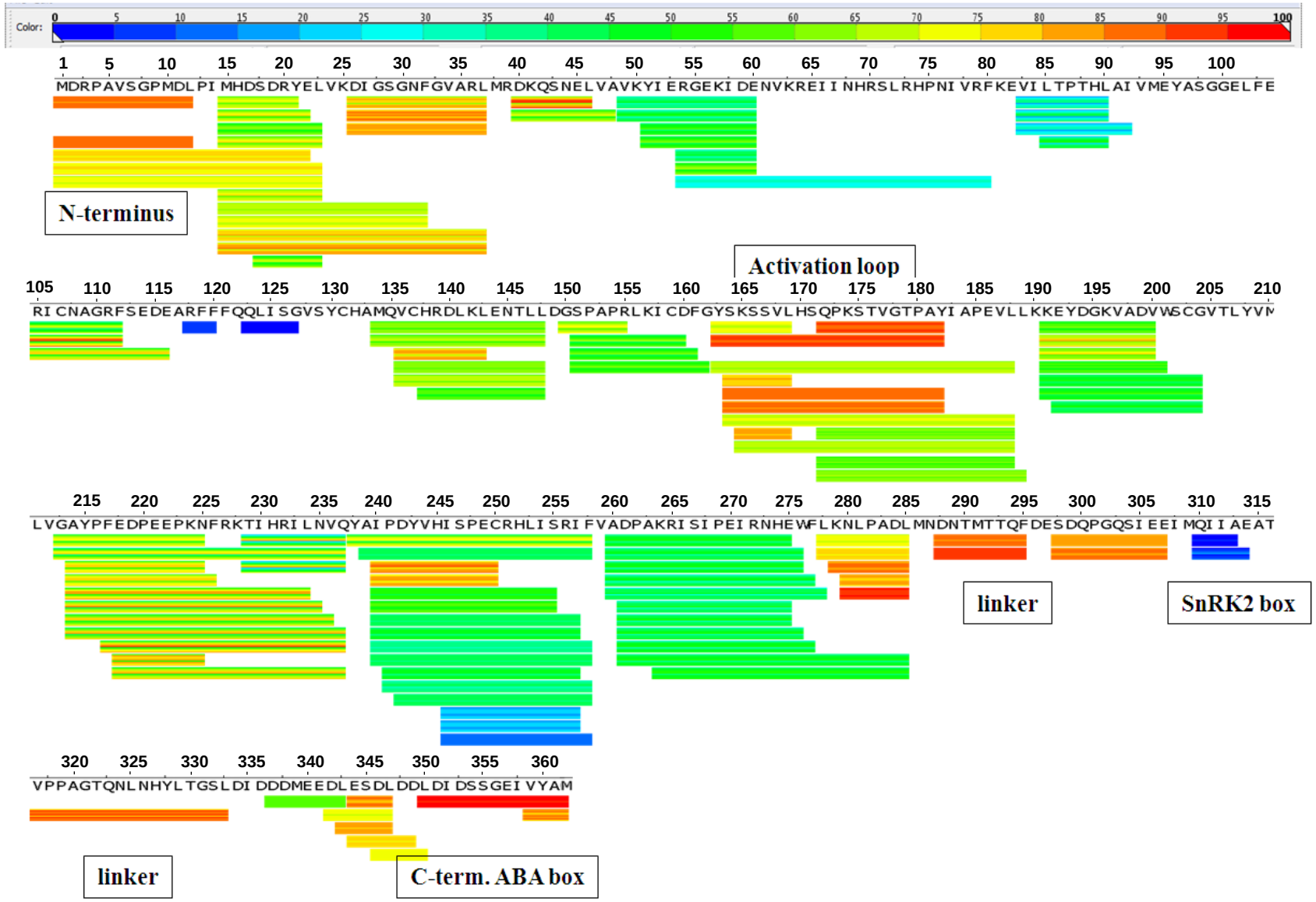

Supplemental Figure 7: HDX protection map of apo SnRK2.6. The bars below the sequence represent the peptide fragments resolved by mass spectrometry and the bar colors represent the relative deuterium/hydrogen exchange (color code on top). Amino acid positions of the SnRK2.6 protein are indicated above the sequence.

Supplemental Fig. 8

A: SnRK2.3

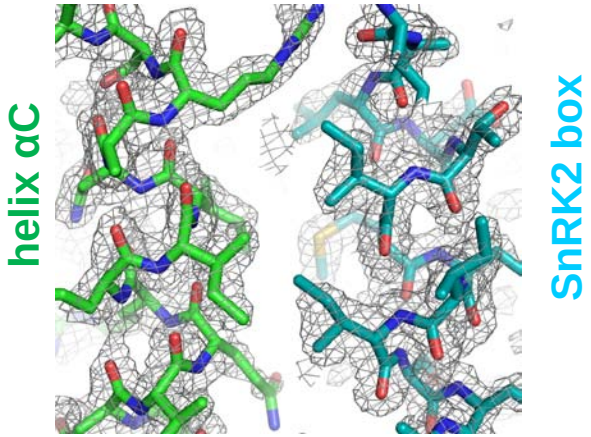

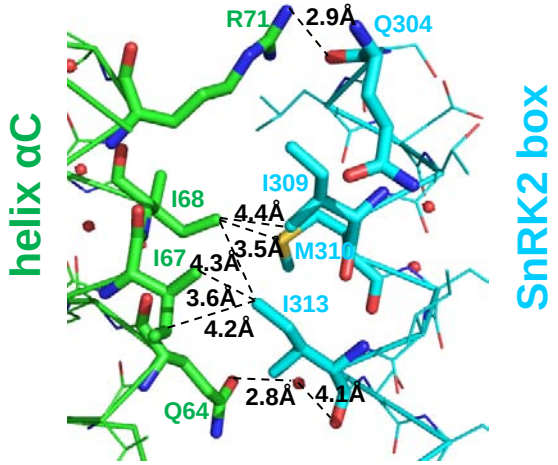

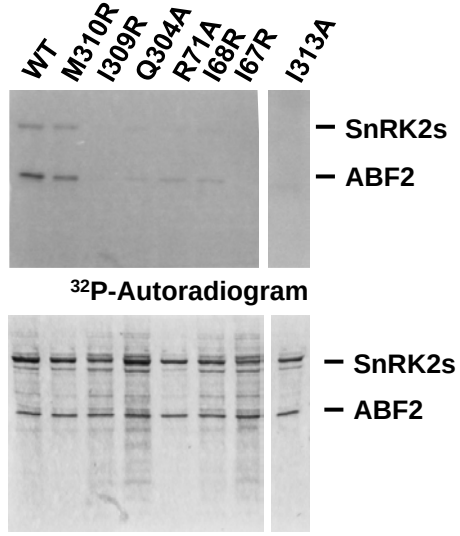

B: SnRK2.6

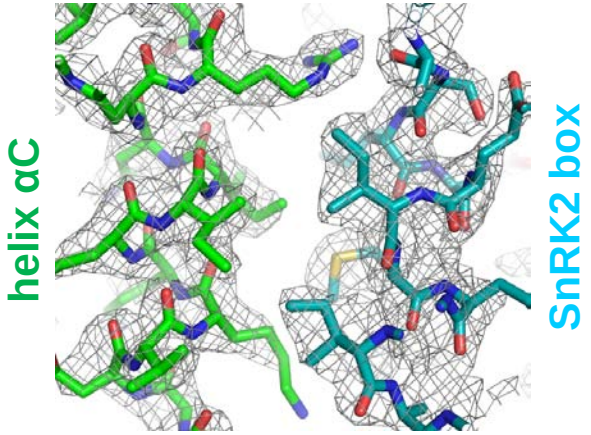

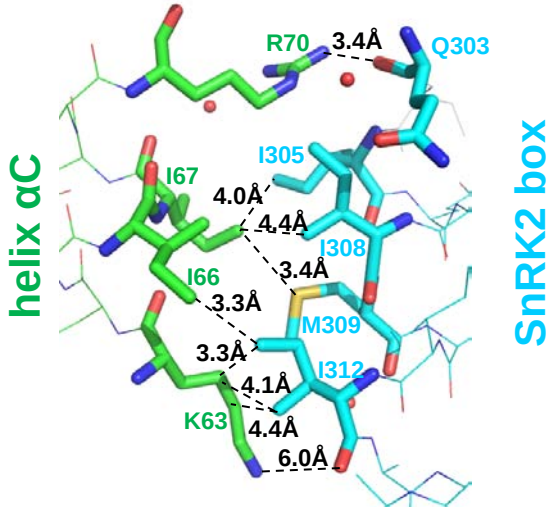

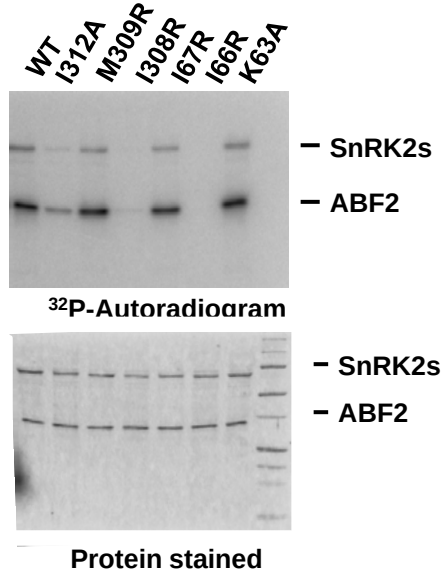

Supplemental Figure 8: The SnRK2 box–αC interaction is required for SnRK2 activity. (*A*) SnRK2.3, (*B*), SnRK2.6 (monomer A). *Left:* $2F_o$-F_c composite omit maps contoured at 1.0σ of the interaction surfaces between αC (green) and SnRK2 box (cyan) helices. *Middle*: SnRK2 box–αC interaction maps. The helices are shown as line presentations with key residues shown as stick models. Water molecules are indicated as red balls and bonds as dashes with distances indicated in Å. *Right*: Kinase assays using wildtype and mutant SnRK2.3 and SnRK2.6.

Supplemental Fig. 9

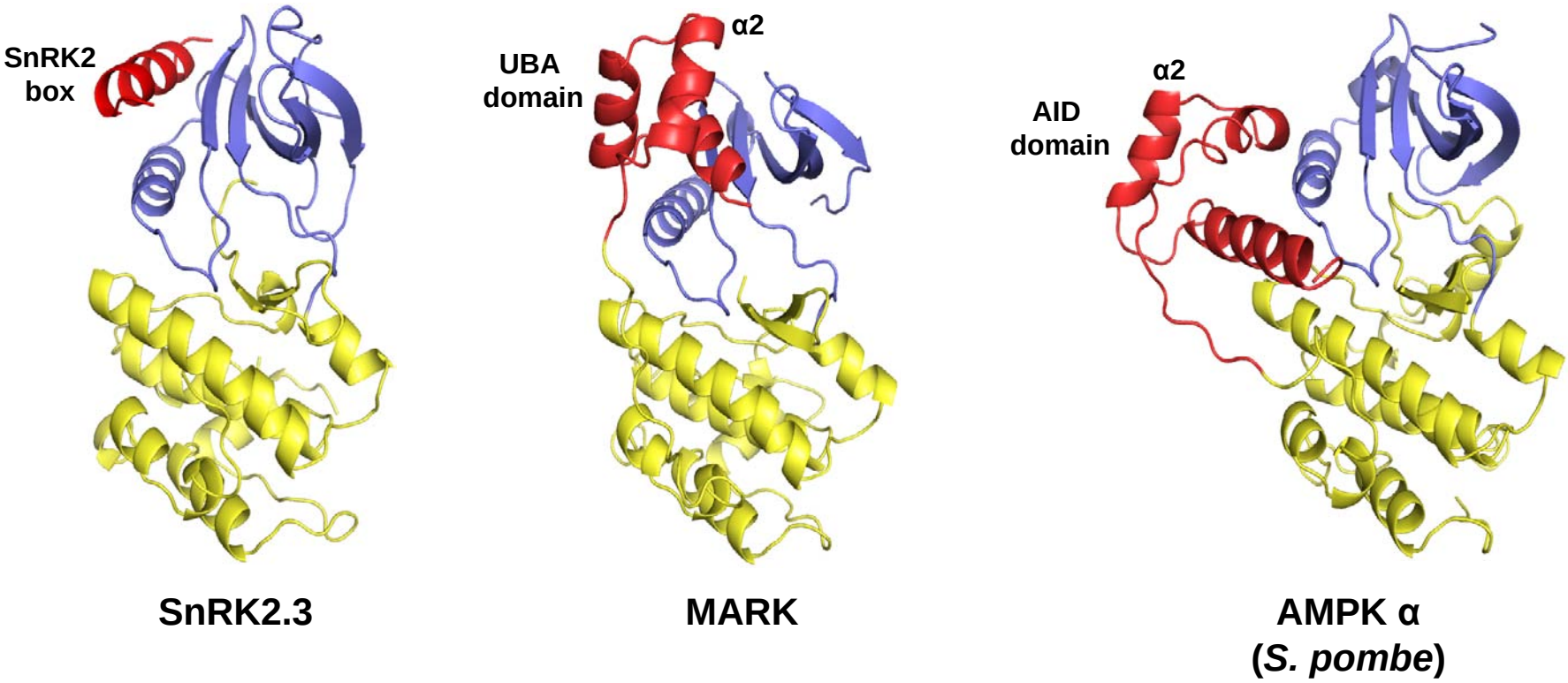

Supplemental Figure 9: Comparison of the SnRK2 box, UBA domain, and AID domain of AMPK-related kinases. Ribbon diagrams with the large and small lobes of the kinase domains shown in yellow and blue and the accessory domains in red.